J. Astrophys. Astr. (2022)43:8
https://doi.org/10.1007/s12036-021-09796-2

ACTIVE GALACTIC NUCLEI

Understanding emission signatures of AGN jets through numerical simulations

SRIYASRITI ACHARYA* and BHARGAV VAIDYA

Department of Astronomy, Astrophysics and Space Engineering, Indian Institute of Technology Indore, Indore 453552, India.
Corresponding author. E-mail: sriya.acharya@gmail.com

MS received 29 July 2021; accepted 16 November 2021

Abstract. The multi-wavelength non-thermal emission from the relativistic AGN jets exhibits flux variability ranging from a very short timescale of minutes, hours to long-timescale of months and years. These magnetically driven jets are subject to several instabilities during their propagation in space. Magneto-hydrodynamical (MHD) instabilities are the most probable candidate responsible for magnetic energy dissipation that could prompt jet radiation and particle acceleration. In this work, we have investigated the impact of the pitch profile and magnetization value on developing the current-driven (CD) kink instability in the moderately relativistic regime of Lorentz factor 5. To achieve this, we simulate a 3D plasma column, a representative section of an AGN jet. From our analysis, a stalled growth of the instability is apparent with a lower magnetization value due to the variable Alfvénic nature of the flow. In addition, we have also investigated the impact of constant pitch profile on the dynamical evolution of the plasma column and the corresponding emission features.

Keywords. Jets—instabilities—non-thermal radiation.

1. Introduction

Relativistic jets are collimated outflows of plasma, often seen in the active galactic nuclei (AGNs) (Urry & Padovani 1995; Blandford *et al.* 2019; Hardcastle & Croston 2020), lie in a direction perpendicular to the plane of the underlying accretion disk. These jets emit non-thermal emission covering the whole gamut of the electromagnetic spectrum starting from radio to γ-rays and being characterized by multi-timescale flux variability. The short variability timescale (being minutes, hours or days) provides information regarding the size of the compact objects and responsible processes for the sudden release of energy causing outburst or flare kind of activity. At the same time, understanding the fundamental physics of variability is only possible by performing a long-term study. Various works have been done to study short timescale events of blazar jets (Begelman *et al.* 2008; Ghisellini & Tavecchio 2008; Gupta *et al.* 2008; Barkov *et al.* 2012), whereas not many studies have been able to explain long-term variability due to observational limitations such as insufficient long-term multi-frequency and simultaneous data.

During their propagation in space, jet instabilities are believed to be one of the plausible mechanisms that play a fundamental role in energy dissipation processes. Several numerical simulations have been performed to understand the effect of magnetohydrodynamical (MHD) instabilities on the jet's morphological properties. Few studies have focused on understanding the impact of these instabilities on emission properties. Previously, Zhang *et al.* (2017) have performed the numerical analysis of kink instability and have found that in the emitting region of blazar jets, the fluctuations observed in the polarization angle may have a kink origin. Recently,

This article is part of the Special Issue on "Astrophysical Jets and Observational Facilities: A National Perspective".

Published online: 12 February 2022

Bodo *et al.* (2021), Kadowaki *et al.* (2021), Medina-Torrejón *et al.* (2021) have suggested that the current sheets generated at the re-connection region due to the kink instability are a possible particle acceleration site. Apart from polarization property, kink may be responsible for the observed quasi-periodic oscillations in blazar jets with the periodicity associated with the growth time of the kink instability (Dong *et al.* 2020).

In particular, the current-driven kink instability causes a transverse deflection of the plasma column with the onset of the instability. Due to bending, it takes the structure of a helical or a curved jet. Further, the presence of a binary black hole system, rotation or twisting of the jet may lead to taking a helical structure. Here, we are interested in analyzing the possible imprint of the kink instability on the jet radiation properties. Recently, Raiteri *et al.* (2017) suggested that a 'helical jet model' provides a possible explanation for the observed long-term variability properties of the blazar jets due to a variable Doppler boosting factor. Noting this Acharya *et al.* (2021) have carried out a parameter survey by performing RMHD simulations of the plasma column with high on-axis magnetization value $\sigma_0 = 10$ and a decreasing pitch profile with a Lorentz factor $\Gamma = 5$ and 10. Their statistical estimates from the synthetic light curves connect the dynamics of the column with the emission features and support the 'helical jet model' as a possible explanation for the long-term flux variation over a time-scale of ≤ 20 years.

This paper investigates the effect of different pitch profiles and magnetization values on the dynamical evolution of the kink instability and its impact on the non-thermal emission signatures of AGN jets.

2. Numerical setup and non-thermal emission modeling

In the present work, the numerical relativistic MHD (RMHD) simulations of plasma column are performed using the PLUTO code (Mignone *et al.* 2007). The computational domain is defined in the Cartesian box of size $8R_j \times 8R_j \times 12R_j$ with 1/60 resolution in all three directions. A constant axial velocity and a zero azimuthal velocity are provided within the radius of the plasma column $R_j = 0.5$, and the ambient medium is considered to be static. We choose a force-free magnetic field as the initial configuration with the radial profile of poloidal and toroidal magnetic field components as follows (Mizuno *et al.* 2011):

$$B_z = \frac{B_0}{\left[1 + \left(\frac{R}{a}\right)^2\right]^{\alpha}}, \tag{1}$$

$$B_\phi = \frac{B_0}{\left(\frac{R}{a}\right)\left[1 + \left(\frac{R}{a}\right)^2\right]^{\alpha}} \sqrt{\frac{\left[1 + \left(\frac{R}{a}\right)^2\right]^{2\alpha} - 1 - 2\alpha\left(\frac{R}{a}\right)^2}{2\alpha - 1}}, \tag{2}$$

where $R = \sqrt{x^2 + y^2}$ is the radial position in a cylindrical coordinate system and B_0 is the magnetic field value at the axis. The magnetic field in the radial direction is $B_r = 0$. Here, α defines the profile of the pitch parameter that is defined as $P = rB_z/B_\phi$ and $a = R_j/2$ is the magnetization radius. An ideal gas equation of state with adiabatic index 5/3 has been considered here.

The magnetization parameter on the axis of the column is given by:

$$\sigma_0 = \frac{B_0^2}{\rho_0},$$

where $\rho_0 = 1.0$ is the density on the axis. Our simulations are carried out with a constant ($\alpha = 1$) and decreasing ($\alpha = 2$) pitch profiles and having typical Lorentz factor $\Gamma = 5$ (plasma column velocity $V_j/c \approx 0.97$). We have chosen two different initial on-axis magnetization values to study the dynamical evolution of the plasma column. The parameter details of the two simulation setups (Ref_s1 and Ref_p1) considered in this work, along with our reference run (Ref), are provided in Table 1. The Ref run is characterized with $\Gamma = 5$ and $\sigma_0 = 10$ with a decreasing pitch profile and the corresponding results are explained in Acharya *et al.* (2021). The radial profile of the magnetic field components, density and the pitch parameter for the Ref and Ref_p1 cases is shown in Figure 1. It should be noted that the radial profile for the Ref_s1 case is similar to the Ref case with a lesser maximum amplitude in the magnetic field components. The initial equilibrium is perturbed by applying a velocity in the radial direction. The detailed particulars about the numerical setups are the same as Acharya *et al.* (2021). To scale the computational units with the physical units, we define three

Table 1. Summary of simulation runs.

Runs ID	σ_0	α
Ref	10.0	2.0
Ref_s1	1.0	2.0
Ref_p1	10.0	1.0

Runs ID, initial magnetization value at the axis (σ_0) and the pitch profile parameter (α).

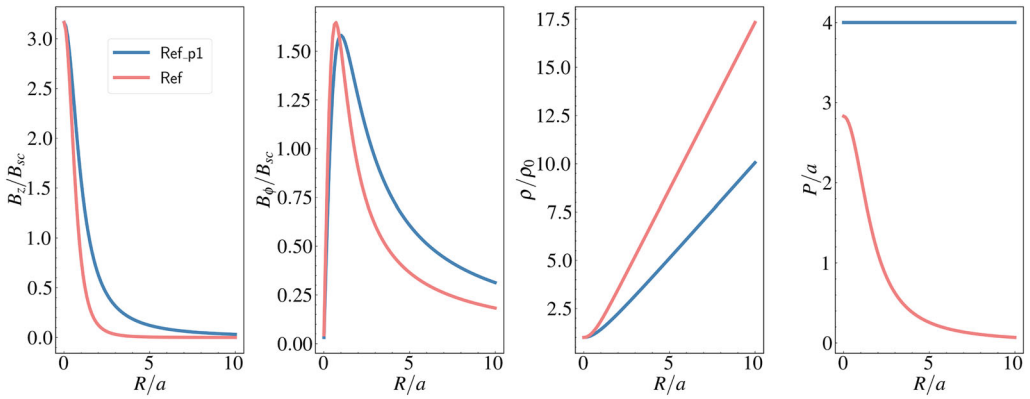

Figure 1. Initial radial profile of axial and toroidal magnetic field components, density and the pitch parameter for the Ref and Ref_p1 cases.

physical scales: the length scale $L_{sc} = 0.1$ pc, the velocity of light $c = 2.998 \times 10^{10}$ cm/s and the density $\rho_0 = 1.673 \times 10^{-24}$ gm/cm^3. As a consequence, the unit for time is $t_{sc} = 0.32$ years, and for the magnetic field is $B_{sc} = 1.374 \times 10^{-1}$ Gauss.

In this work, we estimated the synchrotron emission by considering each grid cell of the computational box as a single emitting blob and study the impact of the different simulation parameters such as σ_0 and α, on the emission signatures of the jets. The synchrotron emission is primarily due to the non-thermal particles with a single power-law particle distribution with index p. The synchrotron emissivity in the observer's frame is calculated by considering the fluid variables as the inputs obtained from the simulations. In this study, we use a static particle spectra with $p = 3$ and the limits of electron energy in the particle spectra is considered to be $\gamma_{\min} = 10^2$ and $\gamma_{\max} = 10^6$. Further, we use the radiative transfer equation to calculate the observed flux density for a particular frequency and viewing angle. The simulated flux density provided here is scaled with $F_{\nu_{sc}}$, that is defined as

$$F_{\nu_{sc}} \approx 4.765 \times \left(\frac{\gamma_{\max}}{10^6}\right)^{-3} \text{ ergs s}^{-1} \text{ cm}^{-2} \text{ Hz}^{-1}.$$

The comprehensive description of the emission modeling approaches and physical scales are provided in Acharya *et al.* (2021).

3. Results

In this work, we have investigated and discussed the impact of lower magnetization value and a constant pitch profile on the dynamical evolution of kink instability in Section 3.1 and its effect on the observed emission features in Section 3.2.

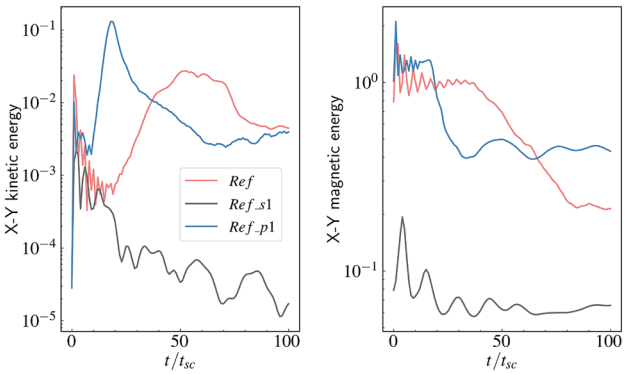

Figure 2. Time evolution of the volume-averaged kinetic and magnetic energies for Ref, Ref_s1 and Ref_p1 cases.

3.1 *Dynamics*

In Figure 2, we show the time evolution of the volume-averaged transverse kinetic and magnetic energies for Ref_p1 and Ref_s1 cases compared with the Ref case as an indicator of the growth of the instability. For the Ref_p1 case, the initial growth phase of the instability is characterized by an exponential increase in kinetic energy until $t/t_{sc} \approx 15$–20 followed by a slow decline in both kinetic and magnetic energies in the non-linear regime. However, as described in Acharya *et al.* (2021), the temporal evolution of energies in Ref_s1 case does not follow the same trend as the Ref_p1 case.

In Ref_p1 case, the development of instability occurs faster compared to the Ref case. During the linear phase ($t/t_{sc} \leq 20$), the kink grows at the

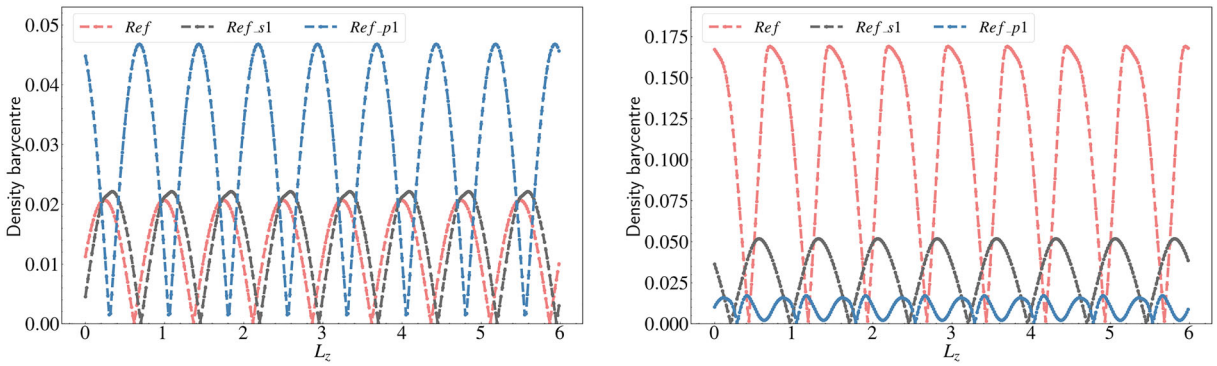

Figure 3. Axial variation of density barycentre for the runs Ref, Ref_s1 and Ref_p1 at $t/t_{sc} = 10$ (left) and $t/t_{sc} = 50$ (right).

boundary of the plasma column, exhibiting ≈ two times the higher displacement of the density barycentre from its axis than the Ref case as shown in the left panel of Figure 3. During the non-linear phase, in Ref_p1 case, the kink grows close to the axis, implying a higher density distribution in that region. This is visible from the right-side panel of Figure 3, where the density barycentre displacement is 6–7 times lower in Ref_p1 case compared to the Ref case, where the kink is still growing at the boundary. In the Ref case, with decreasing pitch profile, the transition to non-linear phase occurs at $t/t_{sc} \approx 50$–55 with a smaller maximum amplitude of transverse kinetic energy. A detailed discussion on the dynamical result of the Ref case is given in Acharya *et al.* (2021).

In the lower magnetization case (Ref_s1), a mixing of both kink and Kelvin–Helmholtz instability is expected as the density-weighted averaged Alfvénic Mach number (M_A) values vary from initially sub-Alfvénic to the later trans-Alfvénic regime. Due to the weak magnetic field strength, a stalled growth of the kink mode is visible in comparison to the higher σ case. This reflects in the right side density barycentre plot as shown in Figure 3. At $t/t_{sc} = 50$, the instability in the Ref and Ref_s1 cases has evolved enough to form a helical structure. However, depending on the growth of the instability, the barycentre displacement for the Ref case is ≈3–4 times higher than the Ref_s1 case.

3.2 *Emission*

To understand the emission properties associated with constant pitch and lower σ configurations, we have estimated the total integrated synchrotron flux at an observing frequency of $\nu_{obs}/\nu_{sc} = 5.09 \times 10^8$, that corresponds to emission in optical (R-Band), where $\nu_{sc} \approx 8.84 \times 10^5$ Hz. The simulated light curves for the Ref_s1 and Ref_p1 cases are shown in Figure 4 for an observer making $\theta = 5°, 20°$ and $45°$ angle with respect to the axis of the plasma column. This section provides a qualitative explanation of the dependence of viewing angle on the emission associated with twisted kinked jets. According to the 'helical jet model', as the jet structure is dynamic, the emitting regions of the jet are different depending on the line of sight of the observer. Therefore, the boosting or diminishing of emission is subject to the orientation of the emitting region of the jet with respect to the viewing angle of the observer. Acharya *et al.* (2021) found that for configurations with high magnetization value and decreasing pitch profile, the growth of the kink instability is enough to take a helically-twisted structure. The temporal variation of spatially integrated synchrotron flux is different for an observer making 5°, 20° and 45° angle with respect to the axis of the plasma column.

However, the temporal variation of spatially integrated flux for the Ref_s1 case does not differ significantly for an observer making 5°, 20° and 45° angle. This suggests that the growth of instability is not sufficient to show any effects of viewing angle on the emission.

In Ref_p1 cases, the onset of the instability occurs at the initial time of the simulation. An appreciable variation can be seen in the integrated flux till $(t - t_{beg})/t_{sc} \leq 20$ (see right panel of Figure 4), where $t_{beg} = 10$. However, in its non-linear phase of evolution, the kink grows close to the axis, indicating less deformation of the plasma column. This results in inappreciable variation in the integrated flux for a different viewing angle of the observer for the duration $(t - t_{beg})/t_{sc} > 20$.

The measure of variability in the simulated flux is quantified through the parameter defined as relative variability amplitude (RVA) or the variability index

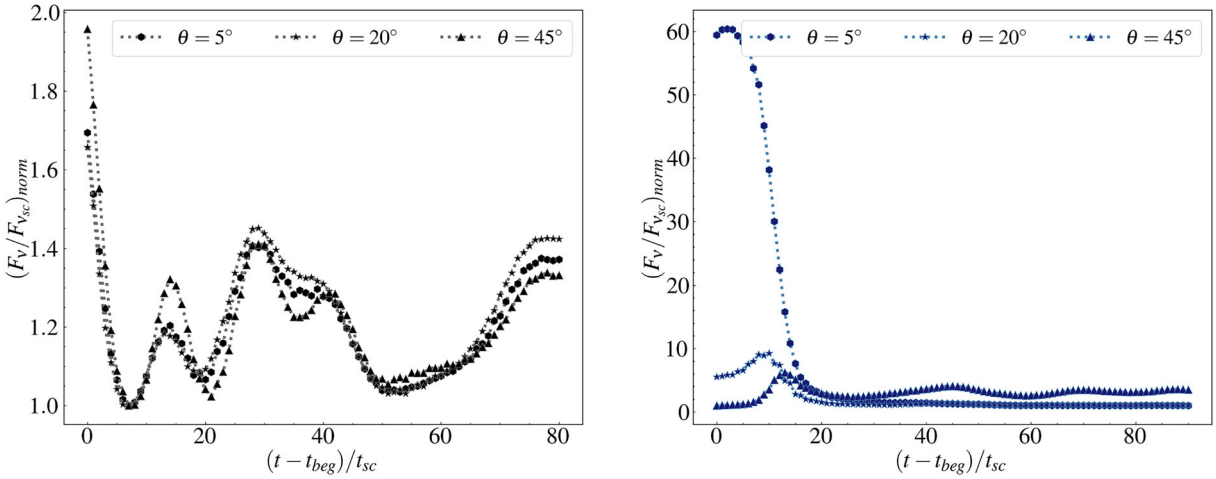

Figure 4. Simulated light curve for the Ref_s1 case in the left panel with $t_{beg} = 20t_{sc}$ and for the Ref_p1 case in the right panel with $t_{beg} = 10t_{sc}$. Here $F_v/F_{v_{sc}}$ is normalized to 2.07×10^{-23}, 6.96×10^{-25} and 7.57×10^{-27} in Ref_s1 case and normalized to 1.24×10^{-23}, 9.61×10^{-24} and 5.02×10^{-25} in Ref_p1 case for $\theta = 5°$, $20°$ and $45°$, respectively.

(Kovalev *et al.* 2005; Singh *et al.* 2019). For the Ref_s1 case, the variability amplitude is found to be 0.25 ± 0.00002, 0.24 ± 0.00005 and 0.32 ± 0.00003 for an observer making 5°, 20° and 45° angle with respect to the axis of the plasma column, respectively. In Ref_p1 case, the variability is found to be maximum for an observer making 5° angle with variability amplitude 0.44 ± 0.00002 for the time $t/t_{sc} > 30$. However, no significant variability is observed for $\theta =$ 20° and 45° during that period with RVA value $0.17 \pm$ 0.00003 and 0.26 ± 0.00003, respectively. During the onset of instability ($t/t_{sc} \leq 30$), the simulated emission exhibits a higher variability amplitude with RVA value 0.89 ± 0.00005, 0.68 ± 0.00005, 0.7 ± 0.00002 for $\theta = 5°$, 20° and 45°, respectively. A high RVA value corresponds to a high growth rate of instability during the early period of the evolution of the plasma column.

4. Discussion and summary

The geometric model is considered as one of the approaches to explain the long-term variability of AGN jets in the presence of a twisted jet. In this model, a change in the jet orientation causes variation in the Doppler factor and hence in the observed flux. In this paper, we have analyzed the effect of the dynamical evolution of the instability on the emission features by performing high-resolution 3D relativistic MHD simulations of a plasma column. The present work aims to validate the physical configurations preferable for forming a twisted helical jet in the context of explaining long-term flux variation. In particular, we perform simulations of kink instability with a constant pitch profile and lower magnetization value. In the Ref_s1 case, mixing of both kink and KH instabilities is expected due to the variable Alfvénic nature of the flow. The stalled growth of the instability gets reflected in the volume-averaged energies and the density barycentre deviation. In Ref_p1 case, during the linear phase of evolution, the kink grows at the boundary of the plasma column. In the non-linear phase, the kink develops near the axis of the column representing the minimal deviation of the density barycentre. In the context of emission, we estimated the synchrotron flux for three different lines of sight of the observer, integrated over the whole plasma column. In both cases, the development of the instability is not sufficient to form a helical structure to show any significant variation in the simulated emission for different viewing angles. In the Ref_p1 case, the statistical estimate suggests variability during the onset period of the instability. In the non-linear phase of evolution in Ref_p1 case, noticeable variability is detected for an observer making 5° angle with respect to the axis of the plasma column compared to 20° and 45° angle. A plasma column with decreasing pitch profile and high magnetization value demonstrates the effect of viewing angle in the context of helical jet model (Acharya *et al.* 2021). These configurations ensure a stronger toroidal magnetic field component compared to the poloidal component, which is considered an integral component for the formation and development of the kink instability. The simulations in Acharya *et al.* (2021) are characterized by different axial wavenumbers of the perturbation (n)

with axial Lorentz factor $\Gamma = 5$ and 10. The case with the lowest n exhibits the maximum growth rate and the maximum variability among the runs. The steady growth of the instability results in a helically structured jet for the values of n that exhibit the dependence of viewing angle on the emission signatures of the jet. Additionally, a correlated trend between the kink growth rate and the observed variability is obtained, where the variability amplitude is maximum for the case with the highest growth rate of the instability. The current results from the dynamical analysis and its associated emission features allow us to particularize the parameters appropriate for developing a well distinct helical jet due to MHD kink instability. This study suggests that the configuration with a lower magnetization value does not favor the explanation for long-term flux variation in the context of the helical jet model. However, with initial constant pitch profile and high magnetization value, there exists variability for a period that corresponds to nearly six years in physical units.

Acknowledgments

The author, SA would like to acknowledge DST INSPIRE Fellowship for the support for PhD. The author, BV would like to acknowledge the support from the Max Planck Partner Group Award. The computations presented here are carried out using the facilities provided at IIT Indore and the Max Planck Institute for Astronomy Cluster: ISAAC.

References

Acharya S., Borse N. S., Vaidya B. 2021, MNRAS, 506, 1862
Barkov M. V., Bosch-Ramon V., Aharonian F. A. 2012, APJ, 755, 170
Begelman M. C., Fabian A. C., Rees M. J. 2008, MNRAS, 384, L19
Blandford R., Meier D., Readhead A. 2019, ARAA, 57, 467
Bodo G., Tavecchio F., Sironi L. 2021, MNRAS, 501, 2836
Dong L., Zhang H., Giannios D. 2020, MNRAS, 494, 1817
Ghisellini G., Tavecchio F. 2008, MNRAS, 386, L28
Gupta A. C., Fan J. H., Bai J. M., Wagner S. J. 2008, AJ, 135, 1384
Hardcastle M. J., Croston J. H. 2020, NAR, 88, 101539
Kadowaki L. H. S., de Gouveia Dal Pino E. M., Medina-Torrejón T. E., Mizuno Y., Kushwaha P. 2021, APJ, 912, 109
Kovalev Y. Y., Kellermann K. I., Lister M. L., *et al.* 2005, AJ, 130, 2473
Medina-Torrejón T. E., de Gouveia Dal Pino E. M., Kadowaki L. H. S., *et al.* 2021, APJ, 908, 193
Mignone A., Bodo G., Massaglia S., *et al.* 2007, APJS, 170, 228
Mizuno Y., Hardee P. E., Nishikawa K.-I. 2011, APJ, 734, 19
Raiteri C. M., Villata M., Acosta-Pulido J. A., *et al.* 2017, NAT, 552, 374
Singh K. K., Meintjes P. J., van Soelen B., Ramamonjisoa F. A., Vaidya B. 2019, APSS, 364, 88
Urry C. M., Padovani P. 1995, PASP, 107, 803
Zhang H., Li H., Guo F., Taylor G. 2017, APJ, 835, 125